ELSEVIER

Physica D 137 (2000) 205–227

PHYSICA D

www.elsevier.com/locate/physd

Disheveled Arnold's cat and the problem of quantum–classic correspondence

S.P. Kuznetsov

Institute of Radio-Engineering and Electronics, Saratov branch, Russian Academy of Sciences, Zelenaya 38, Saratov 410019, Russian Federation

Received 16 November 1998; received in revised form 29 July 1999; accepted 10 August 1999
Communicated by F.H. Busse

Abstract

Quantum Arnold's cat map is studied for a case of perfect square inverse Planck's constant, $N = M^2$. The classic limit is analyzed on a subset of numbers N increasing as 4^k. The quantum problem in this case allows exact reduction to the classic cat map defined on a discrete lattice of size $M \times M$ and supplemented by evolution of a phase variable. A link between the classic periodic orbits and spectrum of eigenvalues of the quantum evolution operator is outlined. For M growing as 2^k genetic analysis is developed for periodic orbits, and they are classified by means of a tree-like graph. A phase shift, accumulated over a period of the orbits, evolves from level to level of the graph according to a certain rule, governed by non-periodic binary code. Representation of a localized Gaussian wave packet in a basis of eigenvectors of the evolution operator gives rise to a probability measure distributed on a unit circle, where the eigenvalues are located. This measure looks like spectrum of a finite-time sample of a stationary random process (periodogram): (1) majority of the eigenstates have intensities of comparable order of magnitude, (2) the spectral distribution is of locally random-like nature, i.e. statistical variance of the amplitudes has the same order as the amplitudes themselves. This combination of properties in very straightforward manner follows from chaotic nature of the classic map and is conjectured to be the most fundamental attribute of quantum chaos.

PACS: 05.45.+b, 03.65.Sq

Keywords: Quantum map; Quantum chaos; Classic limit; Correspondence principle

1. Introduction

It is known that classic nonlinear systems can manifest dynamical chaos. However, on a fundamental level we must use quantum, not classic mechanics. What is chaos from the quantum-mechanical point of view? This question is a subject of an extensive and developing scientific discipline called 'quantum chaos' or, after Berry, 'quantum

E-mail address: kuz@spkuz.saratov.su (S.P. Kuznetsov).

0167-2789/00/$ – see front matter
PII: S0167-2789(99)00182-7

chaology' [1–12]. Paradoxically, its starting point is an assertion that chaos, in the usual sense, cannot occur in quantum dynamics associated with finite motion of a system isolated from the rest world. This circumstance looks like apparent contradiction challenging the correspondence principle, which declares that the theory must have the classic mechanics as a limit case [13]. It is a basic problem of quantum chaology to consider carefully the process of passage to the classic limit, explain originating chaos in this process, and clear up contents, which we have to put into the correspondence principle.

While speaking of classic chaos, it is proved fruitful to study artificial simple models,such as baker's map or a family of linear hyperbolic automorphisms of torus called 'the cat maps' [6,14,15]. It is reasonable to assume that quantum counterparts of the named models should play comparably important role in the quantum chaology. Exploitation of this idea started from seminal work of Hannay and Berry [16], where a definite quantization procedure for linear maps on torus was introduced, conditions of its validity were stated, dynamics of quantum analogs of maps with chaotic and regular dynamics were studied and compared. Since then, many authors studied quantum analogs of simple chaotic maps [16–38]. In particular, for the cat maps structure of eigenvectors was revealed, which may be random-like or regular [3,19,34]; quantum analogs of Lyapunov exponent, ergodicity and mixing were discussed [26,36,37]; some alternative quantization schemes were suggested [17,27,38]. Spectral distribution of quasi-energies was investigated in detail by Keating [21,22] with the help of an appropriate version of the trace-formula. This distribution was found to be very special, distinct from those intrinsic to typical quantum chaotic systems and random matrix ensembles. (To restore generic behavior some perturbation producing more general nonlinear Anosov map should be done in the original cat map [31,32].) Importance of a question on quantum-classic correspondence is commonly recognized, and it is touched in a majority of the mentioned works. Papers of Ford et al. [17,18] are devoted specially to this problem, and the authors stress its subtlety and non-triviality.

Discussing quantum maps on torus one has to account that only such values of the Planck's constant are allowed, which satisfy the relation [16–22]:

$$\hbar = (2\pi N)^{-1}. \tag{1}$$

Here periods of the phase space in respect to coordinate x and momentum p are normalized to unity, and N is an integer parameter, which controls relative significance of quantum effects.

According to Eq. (1), the classic limit $\hbar \to 0$, in principle, may be considered only in a restricted sense, like a partial limit, because we cannot handle $\hbar$ as a continuous variable. If all integers $N = (2\pi\hbar)^{-1}$ are taken into account, the passage to the limit looks very complicated and irregular: it reflects all number-theoretic properties of the natural numbers (such as distribution of primes and so forth) [16,21–24]. From the other hand, being forced in any case to work with a discrete set of $\hbar$, why could not we make further restriction and take a subset with simpler regular structure? It may be hoped that the passage to the limit becomes then more transparent and allows better understanding the nature of the quantum–classic correspondence.

Development of this approach is the basic aim of this article. We will take a set of numbers N growing as 4^k and consider a quantum analog of one particular representative of the cat maps, namely

$$p_{t+1} = p_t + x_t, \quad x_{t+1} = p_t + 2x_t \pmod 1. \tag{2}$$

This is just the map originally suggested by Arnold [14,15,17]. Illustrated by a picture of the cat face it gave name to the whole family.

Section 2 shortly reproduces derivation of quantum evolution operator of the Arnold's cat map for even N [17]. Then we exploit the fact that the numbers $N = 4^k$ are perfect squares and suggest in Section 3 a special representation of the quantum problem appropriate for $N = M^2$. Based on a version of Fourier-like transformation invented by Gelfand [39–41] this representation allows such quantum states that move like classic particles on a discrete lattice of size $M \times M$, and this motion is supplemented by a phase variable, like in the 'old' quantum

mechanics. In Section 4 a link between classic periodic orbits and eigenstates of the quantum evolution operator is discussed. In Section 5 the orbits on the lattice $M \times M$, $M = 2^k$ are enumerated and classified genetically by means of a tree-like graph. In Section 6 we calculate an important factor responsible for mutual ordering of eigenvalues associated with different periodic orbits and demonstrate irregular nature of its evolution in process of passage to the classic limit. Spectrum of eigenvalues for the case of interest, $N = 4^k$, is discussed in Section 7. In Section 8 we consider representation of a Gaussian wave packet in a basis of eigenvectors of the quantum Arnold's cat map and obtain the corresponding spectral intensity distribution, that is a probability measure defined on a unit circle, where the eigenvalues of the evolution operator are located. In Section 9 several statistical procedures are used to test and illustrate statistical properties of these distributions.

2. Quantum evolution operator for the Arnold's cat map

Classic Arnold's cat map may be presented as a mechanical model [17]. Let we have a particle of unit mass, which moves in one dimension without friction and undergoes a sequence of kicks of unit time period. Intensity of a kick is supposed to be proportional to instantaneous coordinate of the particle. Let position and momentum just before a kick be x_t and p_t, then, after the kick, we have $p' = p_t + x_t$. Next, during the unit time interval, the particle moves freely with the accepted velocity. Just before the next kick momentum equals $p_{t+1} = p' = p_t + x_t$ and position is $x_{t+1} = x_t + p' = p_t + 2x_t$. Finally, we postulate periodicity of the phase space (with unit period along both axes x and p) and arrive to the map (2).

In a quantum system the requirement that wave function has unit period along x-axis means that its Fourier transform (the momentum representation of the wave function) looks like a comb of delta-spikes. Their spacing on the axis of wave number equals 2π, so, in terms of momentum, $\Delta p = 2\pi\hbar$. The only possibility to have unit period along the p-axis is that this period contains an integer number of steps Δp, namely N, and we come to the condition (1).

Being given an N-dimensional vector of complex coefficients at the delta-spikes, Ψ_m, one can construct the quantum map as the following sequence of operations:

1. Multiplication by $\hat{V} = \exp(\mathrm{i}\pi m^2/N)$ accounts a kick. (Action of a potential $U(x)$ for a short time interval Δt corresponds to multiplication of the wave function by $\exp((\mathrm{i}/\hbar)U(x)\Delta t)$, and we have to substitute here $\hbar = (2\pi N)^{-1},\ U(x)\Delta t = x^2/2,\ x = m/N$.)
2. Discrete Fourier transformation

$$\tilde{\Psi}_k = \hat{F}\Psi_m = \frac{1}{\sqrt{N}} \sum_{m=0}^{N-1} \Psi_m \exp(-2\pi \mathrm{i} mk/N)$$

   ensures passage to the momentum representation.
3. Multiplication by $\hat{V}^+ = \exp(-\mathrm{i}\pi k^2/N)$ accounts motion of the particle during an interval between two kicks. (In the momentum representation the free motion corresponds to multiplication of the wave function by $\exp(-\mathrm{i}p^2 t/2m_0\hbar)$, where m_0 is the mass of the particle and t is the duration of the motion. We have to substitute here $\hbar = (2\pi N)^{-1},\ p = k/M,\ t = 1,\ m_0 = 1$.)
4. Inverse Fourier transformation

$$\Psi_m = \hat{F}^+\tilde{\Psi}_k = \frac{1}{\sqrt{N}} \sum_{k=0}^{N-1} \tilde{\Psi}_k \exp(2\pi \mathrm{i} mk/N)$$

   returns us to the initial position representation.

So, the evolution operator over one time step is $\hat{U} = \hat{F}^{+}\hat{V}^{+}\hat{F}\hat{V}$. Its matrix elements may be written explicitly as

$$U_{mn} = \frac{1}{\sqrt{N}} \exp\left(\frac{2\pi \mathrm{i}}{N}(m^2/2 - mn + n^2) - \frac{\pi \mathrm{i}}{4}\right), \quad m, n = 0, 1, \ldots, N-1. \tag{3}$$

Expression (3) coincides (up to complex conjugation) with that found by Ford et al. [17]. As they have mentioned, this form is valid only for even N, because in the other case the quantum evolution destroys the supposed periodicity of the wave functions. Modification appropriate for odd numbers N is suggested in [38] (see also [27]). The necessity to study separately the cases of even and odd N arises because the Arnold's cat map (2) does not relate to the class of maps quantizable according to Hannay and Berry [16,22,27].

3. Gelfand's representation of quantum map for $N = M^2$, its link with the classic map, and the stage of 'disheveled cat'

Let us introduce a special representation of the quantum problem appropriate for a case of perfect square numbers N. It is based on a discrete version of the Fourier-like transformation suggested by Gelfand in 1950 [39].

For a function $f(x)$ on the real axis x the forward and inverse Gelfand's transformations are defined as

$$\tilde{f}_\beta(x) = \sum_{n=-\infty}^{\infty} f(x + nd)\, \mathrm{e}^{-\mathrm{i}\beta n d}, \quad f(x) = \frac{d}{2\pi}\int_0^{2\pi/d} \tilde{f}_\beta(x)\, \mathrm{d}\beta, \tag{4}$$

where d is a constant [39–41]. It is supposed that the infinite sum converges. The transform $\tilde{f}_\beta(x)$ is a function of two variables, x and β, which satisfies the following relations:

$$\tilde{f}_\beta(x + d) = \tilde{f}_\beta(x)\, \mathrm{e}^{\mathrm{i}\beta d}, \quad \tilde{f}_{\beta + 2\pi/d}(x) = \tilde{f}_\beta(x). \tag{5}$$

So, it is sufficient to define the function $\tilde{f}_\beta(x)$ in a rectangular domain $0 \le x < d$, $0 \le \beta < 2\pi/d$.

Gelfand's transformation leads to a very elegant formulation of the Floquet theory and is applicable for such problems as waves in periodic media, parametric resonance, and so forth. Unfortunately, the work of Gelfand did not attract attention of physicists in proper time.

To construct a discrete version of the transformation (4) let us suppose that $N = M^2$ and Ψ_m is an N-dimensional vector. Then we define the forward and inverse transformations

$$w_{ml} = \frac{1}{\sqrt{M}} \sum_{k=0}^{M-1} \Psi_{m+kM}\, \mathrm{e}^{-2\pi \mathrm{i} kl/M}, \quad \Psi_{m+kM} = \frac{1}{\sqrt{M}} \sum_{l=0}^{M-1} w_{ml}\, \mathrm{e}^{2\pi \mathrm{i} kl/M}. \tag{6}$$

The value w_{ml} may be regarded as the discrete version of Gelfand's transform. It depends on two integers m, l, defined modulo M, and satisfies the relations

$$w_{m+M,l} = w_{ml}\, \mathrm{e}^{2\pi \mathrm{i} l/M}, \quad w_{m,l+M} = w_{ml}. \tag{7}$$

Now let us have the quantum Arnold's cat map, and w_{ml} is Gelfand's transform for an initial state vector. What will be result of its evolution after one time step? First, we have to express Ψ_m via w_{ml}, then act by the matrix $\hat{U}$, and finally, return to Gelfand's representation. After some algebra, we obtain

$$w'_{m'l'} = \frac{1}{\sqrt{M}} \sum_{m=0}^{M-1} \sum_{l=0}^{M-1} U_{m',l';m,l}\, w_{ml}, \tag{8}$$

$$U_{m',l';m,l} = \frac{1}{\sqrt{M}} \sum_{\chi=0}^{M-1} \sum_{k=0}^{M-1} \exp\left[\frac{2\pi \mathrm{i}}{M} \chi (m' - m - l') + \pi \mathrm{i} \chi^2 + \frac{2\pi \mathrm{i}}{M} k(-m' + 2m + l) \right]. \tag{9}$$

Note that the term $\pi \mathrm{i} \chi^2$ in the exponent may be changed to $\pi \mathrm{i} \chi$ because only oddness or evenness of χ is relevant here. Then, the sums over χ and k can be evaluated, and the result is

$$U_{m',l';m,l} = \exp\left[\mathrm{i} \frac{\pi}{M^2} (m'^2 - 2m'm + 2m^2) - \mathrm{i} \frac{\pi}{4} \right] \delta_{m',2m+l} \delta_{l',m+l+M/2}. \tag{10}$$

On the basis of Eq. (10) we can interpret dynamics of the quantum system in the following way. Let us consider two-dimensional square lattice of size $M \times M$ with sites enumerated by integer pairs (l, m). To define a state of the quantum system, we attribute a complex number to each site. (It is consistent with Hilbert space dimension of the system, which is $N = M^2$.)

Let us have the unit value at one site (l, m) and zero values at other sites. Then, the position with non-zero amplitude will move along the orbit governed by a map

$$m_{t+1} = 2m_t + l_t, \quad l_{t+1} = m_t + l_t + M/2 \pmod{M}, \tag{11}$$

and this dynamics will be accompanied by evolution of the phase variable according to the equation

$$\varphi_{t+1} = \varphi_t + \frac{2\pi}{M^2} (m_{t+1}^2/2 - m_{t+1} m_t + m_t^2) - \frac{\pi}{4}. \tag{12}$$

Eq. (11) may be rewritten to have the same form as the classic map because the term $M/2$ may be removed by a shift of origin. Setting $P = l - M/2$, $X = m - M/2$, we have

$$P_{t+1} = P_t + X_t, \quad X_{t+1} = P_t + 2X_t \pmod{M}. \tag{13}$$

With additional normalization of the variables $x = X/M$, $p = P/M$ we obtain exactly Eq. (2).

Note that the phase shift (12) is proportional to mechanical action along the classical orbit. Further, we will refer to the term 'action' meaning simply the value of the phase shift measured in units of 2π and designated as $S_t = \varphi_t/2\pi \pmod 1$.

In general, any state of the quantum system may be thought as a superposition of states corresponding to motion along possible orbits with different starting points on the lattice. In particular, we can illustrate quantum dynamics as Arnold does for the classic map [1,14,17]. Let us attribute fixed non-zero value to sites of the lattice inside the contour of the cat's face, and zero values to other sites. Then, we trace evolution according to Eqs. (11) and (12), and plot a little arrow of proper direction at each site where the amplitude is non-zero (Fig. 1). The lattice contains a finite number of sites, so there is a finite time of return, when the cat's face arises again. However, the distribution of phases does not reproduce the initial one, and the cat appears to be 'disheveled'. To observe real quantum return one should wait much longer; it occurs only at the Mth emergence of the cat's face. This complete return corresponds to the Heisenberg time of our system T_{H}.

4. From classical periodic orbits to eigenvectors and eigenvalues of quantum problem

On the lattice of size $M \times M$ the map (11) has a number of periodic orbits (cycles). We shall see that each orbit gives rise to a set of T eigenvectors, where T is a period of the cycle. Indeed, let us have a point of a given periodic orbit (m_0, l_0), and define initial state of the quantum system as $w_{ml} = \delta_{m,m_0} \delta_{l,l_0}$. After T time steps we have

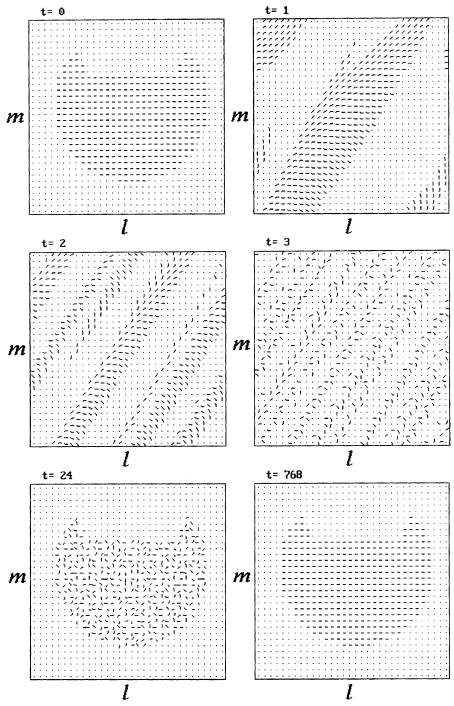

Fig. 1. Dynamics of quantum Arnold's cat map in Gelfand's representation for $N=M^2=1024$. Instantaneous state is given as a set of complex numbers attributed to sites of the lattice $M \times M$. In initial state, at $t=0$, all sites inside the contour of cat face have the same real values, and are zero outside the contour. Motion of the points is governed by mapping (11), and phase variable evolves according to Eq. (12). For $t=24$ a picture of 'disheveled' cat is observed. Complete return to the initial state occurs at $t=768$.

$w_{ml} = \delta_{m,m_0}\delta_{l,l_0}\,\mathrm{e}^{2\pi\mathrm{i}S_T}$, where S_T is the action accumulated along the orbit. The combination $w_{ml}\exp(-2\pi\mathrm{i}S_T t/T)$ depends on t periodically, so Fourier transformation may be done:

$$w^{(r)}_{ml} = \frac{1}{\sqrt{T}}\sum_{t=0}^{T-1}\left(w_{ml}\,\mathrm{e}^{-2\pi\mathrm{i}S_T/T}\right)\mathrm{e}^{-2\pi\mathrm{i}rt/T} = \frac{1}{\sqrt{T}}\sum_{t=0}^{T-1}\delta_{m,m_t}\delta_{l,l_t}\exp\left[\frac{2\pi\mathrm{i}(S_T+r)}{T}t + 2\pi\mathrm{i}S_t\right]. \tag{14}$$

This is an eigenvector in Gelfand's representation with eigenvalue

$$\lambda_r = \exp\left[\frac{2\pi\mathrm{i}(S_T+r)}{T}t\right]. \tag{15}$$

Note that all eigenvalues lie on the unit circle. After return to standard position representation by means of Eq. (6) we obtain from Eq. (14)

$$\Psi^{(r)}_{m+kM} = \frac{1}{\sqrt{M}}\sum_{l=0}^{M-1} w^{(r)}_{ml}\,\mathrm{e}^{2\pi\mathrm{i}kl/M} = \frac{1}{\sqrt{MT}}\sum_{t=0}^{T-1}\delta_{m,m_t}\exp\left[-\frac{2\pi\mathrm{i}(S_T+r)}{T}t + 2\pi\mathrm{i}S_t\right]. \tag{16}$$

Index r enumerates eigenvectors associated with the given periodic orbit. To designate vectors generated by other orbits one more superscript, a Greek letter, will be supplemented.

If all periodic orbits of the classic map on the lattice $M \times M$ are found, the above procedure allows obtaining complete orthonormal basis of eigenvectors and complete spectrum of eigenvalues. The orthoganality relations in Gelfand's representation are

$$\sum_{m=0}^{M-1}\sum_{l=0}^{M-1} w_{ml}^{*(\mu,r)} w_{ml}^{(\nu,s)} = \delta_{\mu\nu}\delta_{rs}. \tag{17}$$

For vectors, generated by different periodic orbits, it follows simply from the fact that the cycles do not have common points. For distinct vectors generated by the same orbit relation (17) is derived from the properties of discrete Fourier transformation.

Evolution of any arbitrary initial state w_{ml}^0 may be easily considered if we represent w_{ml}^0 as a linear combination of the eigenvectors. Indeed, let us set

$$w_{ml}^0 = \sum_{\nu}\sum_{r} C^{(\nu,r)} w_{ml}^{(\nu,r)}, \tag{18}$$

then

$$w_{ml}(t) = \sum_{\nu}\sum_{r} C^{(\nu,r)} w_{ml}^{(\nu,r)} (\lambda_r^{(\nu)})^t. \tag{19}$$

To find the coefficients we multiply Eq. (18) by $(w^{(\mu,s)})^*$ and perform summation over m and l taking into account the orthogonality relations. The result is

$$C^{(\mu,s)} = \frac{1}{\sqrt{T}} \sum_{t=0}^{T-1} w_{m_t,l_t}^0 \exp(2\pi \mathrm{i}(st/T - S_t^{(\mu)} + S_T^{(\mu)} t/T)). \tag{20}$$

5. The case $M = 2^k$: genetic analysis of periodic orbits and tree-like graph

Let us start now the planned program — analysis of passage to the limit $N \to \infty$ on a set of numbers growing as $N = 4^k$.

To solve the quantum problem for $N = M^2$ one has to study orbits of the classic cat map on the lattice $M \times M$. For the case of interest, $N = 4^k$, we may start from $M = 2$ and increase the number step by step to obtain $M = 4, 8, \ldots, 2^k$.

Suppose there is an orbit on the lattice $M \times M$, which runs over sites (P_t, X_t), $0 \le t < T$. Let us take the lattice of doubled size, $2M \times 2M$, and consider the following set of points:

$$D_0 = (P_t, X_t), \quad D_t = (P_t, X_t + M), \quad D_2 = (P_t + M, X_t), \quad D_3 = (P_t + M, X_t + M), \tag{21}$$

where $0 \le t < T$, and sums are defined modulo $2M$. Orbits on a new lattice, which contain points from this set, we call *daughter orbits* for the original *mother orbit*.

For small M it is easy to look through all the orbits and order them by means of a tree-like graph (Fig. 2). After several steps the game rules become evident. Only two top levels are arranged in non-standard manner. The fixed point (0, 0) gives rise to a period-3 cycle containing sites (0, 1) and (1, 1). In turn, this cycle generates four period-3 cycles; their starting points may be taken as (0, 1), (1, 2), (1, 1), and (1, 3), respectively. From this level, the graph has a simple structure of binary tree, and each new level corresponds to doubling of time period in comparison with the previous level. It may be proven using the following reasoning.

From Eq. (13) one can see that the value

$$I = X^2 - XP - P^2 \pmod{M} \tag{22}$$

is an invariant of the mapping conserved during iterations [17]. So, I must be the same for all sites of one periodic orbit, and sites with distinct values of I cannot belong to this orbit.

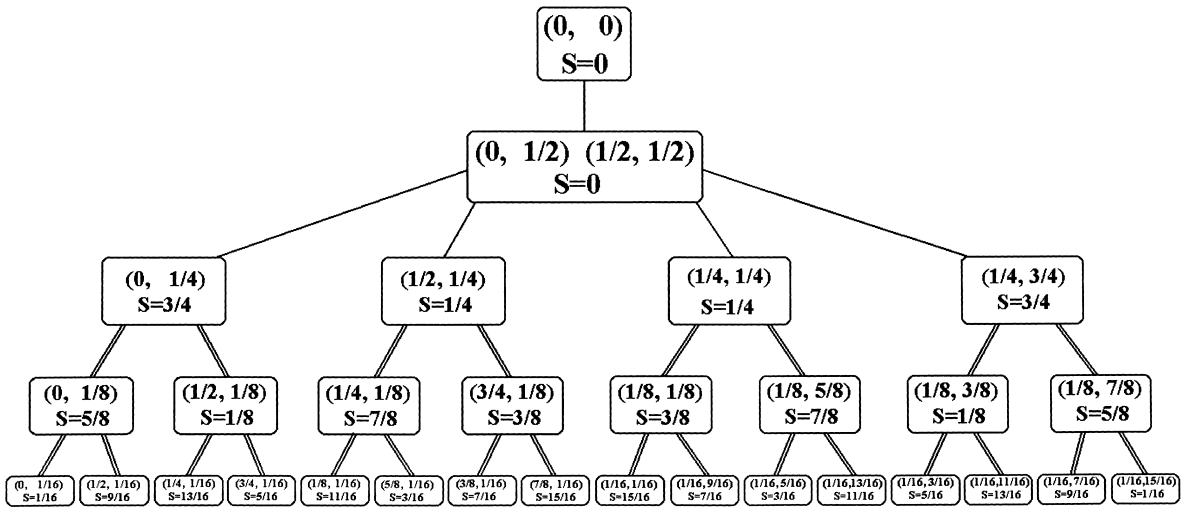

Fig. 2. Graph which arranges periodic orbits of the classic map for $M = 2^k$. Levels from zero to the fourth are shown. Inside each box we present starting point (p_0, x_0) for the corresponding orbit of the map and the value of action S over a period of this orbit. The fixed point occupies zero level, period-3 cycles live on the first and second levels. Double-line edges of the graph designate period doubling.

While building a new level of the graph, we have starting points for mother orbits with odd P, or odd X, or both of them. (Pairs of even P and X correspond to orbits accounted on previous levels of the construction.) According to new value of the invariant I, the points D are separated in the following way:

1. For even P and odd X there are two pairs (D_0, D_1) and (D_2, D_3).
2. For odd P and even X there are pairs (D_0, D_2) and (D_1, D_3).
3. For odd P and odd X there are pairs (D_0, D_3) and (D_1, D_2).

Each pair has a definite value of $I \pmod{2M}$ for the opposite pair it differs by addend M.

It is convenient to normalize variables as $p_t = P_t/M$ and $x_t = X_t/M$. In this notation, the coordinates remain unchanged for all levels already built in a course of subsequent steps of doubling. For daughter orbits coordinates of starting points are expressed via the mother's (p, x) by the following rule:

$$(p, x)_{\text{mother}} \to (p/2, x/2), ((p+1)/2, x/2) \text{ in the left half of the graph,} \tag{23}$$

$$(p, x)_{\text{mother}} \to (p/2, x/2), (p/2, (x+1)/2) \text{ in the right half of the graph.} \tag{24}$$

For given $M = 2^k$ the last level of the graph is occupied by cycles of maximal period $T = \frac{3}{4}M$. One of these cycles, starting at the point $p = 0$, $x = 1/M$ (i.e. $P = 0$, $X = 1$), will be called *the fundamental orbit of the level k*. Note that time $T = \frac{3}{4}M$ corresponds to appearance of disheveled cat face in Fig. 1, and Heisenberg time is $T_{\text{H}} = MT = \frac{3}{4}N$.

6. Explicit expression for action: a map and symbolic dynamics for factor R under subsequent doubling of the lattice size

Let us have $M = 2^k$ and consider an orbit of the map $P_{t+1} = P_t + X_t$, $X_{t+1} = P_t + 2X_t \pmod{M}$, which starts at (P_0, X_0), belongs to the kth level of the graph, and has period $T = \frac{3}{4}M$. Rewriting Eq. (12) via P and X, we obtain the phase shift accumulated over one period

$$\Delta\varphi = 2\pi S_T(P_0, X_0) = \frac{2\pi}{M^2}\sum_{t=0}^{T-1}\left(X_{t+1}^2/2 - X_{t+1}X_t + X_t^2 - X_t M/2\right). \tag{25}$$

From this expression and from linearity of the map (13) it follows that action S_T has quadratic dependence on (P_0, X_0). Moreover, the value of S_T must be the same for all possible starting points on the given periodic orbit. These are just the properties of the invariant I (see Eq. (22)). Apparently, S_T may differ from I only by a factor R_k, which is common for all orbits of the level k. Hence,

$$S_T = R_k(X^2 - XP - P^2), \tag{26}$$

where the constant R_k is the value of action for the fundamental orbit, $R_k = S_T(0, 1) = S_T^0$.

It is shown in Appendix A that for $M = 2^k \geq 8$ the following explicit formula for R_k is valid:

$$R = \left\{\frac{(M/2)+1}{M^2}(F_{T+1} - F_{T-1})\right\} = \left\{\frac{(M/2)+1}{M^2}F_T\right\}, \quad M = 2^k,\ T = \tfrac{3}{4}M, \tag{27}$$

where braces designate the fractional part, and F_i means the ith term of the Fibonacci sequence.

The factor R_k is of crucial importance for arrangement of the quantum dynamics. Via Eqs. (15) and (26) it determines ordering of eigenvalues which are associated with orbits of the kth level. Information about development of the quantum dynamics in a process of passage to the classic limit ($M = 2^k \to \infty$) is hidden in the dependence of the factor R_k on a subscript k.

For $M = 2, 4, 8, 16, 32, 64, \ldots$, one can obtain numerically by Eq. (25), or analytically by Eq. (27) the following sequence of R_k:

$$0, 3/4, 5/8, 1/16, 25/32, 9/64, 105/128, 169/256, 297/512, 41/1024, 553/2048, 3625/4096, \ldots$$

It may be found that a step from $M = 2^k$ to $M = 2^{k+1}$ obeys the rule

$$R_{k+1} = \begin{cases} (\{R_k + 1/2\} + 1)/2, & \sigma_k = 0, \\ \{R_k + 1/2\}/2, & \sigma_k = 1, \end{cases} \tag{28}$$

where σ_k are subsequent symbols of the code [1]

$$\{\sigma_i\} = 0110100011011101001010111110100100000010101010100010011111111$$
$$0111010000000110110111100101101011001101100001010000011110 1\ldots \tag{29}$$

(The first symbol 0 corresponds here to a step from $M = 2$ to $M = 4$.)

Iteration diagram for R_k is presented in Fig. 3. Since $dR_{k+1}/dR_k = 1/2 < 1$, the character of dynamics is determined completely by the code σ_k. From Eq. (27) one can see that it is simply the tail of the binary representation for $F_{3\cdot 2^{k-2}}/2^{2k+1}$. (It may be shown that this tail is stabilized in the limit $k \to \infty$.) The factor of growth for Fibonacci numbers is irrational $w = (\sqrt{5}+1)/2$. Hence, the code cannot be periodic. On the other hand, in the classic Arnold's cat map irrationality of the eigenvalue w^2 associated with positive Lyapunov exponent $\Lambda = \log w^2$ is responsible for appearance of mixing, the essential attribute of the classic chaos [14,15]. We conclude that the mixing property of the classic map and non-periodic, non-regular behavior of R_k, which reflects complicated nature of approach of the quantum map to the classic limit, are manifestations of the same entity.

[1] To obtain the code sequence (29) with many digits, one can use formula (27) together with the doubling algorithm for Fibonacci numbers given in Appendix A.

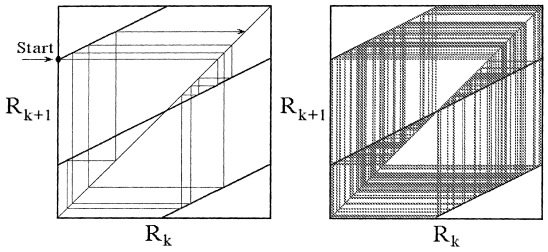

Fig. 3. Iteration diagram illustrating irregular character of the passage to the classic limit under multiple doubling of M. The factor R_k has a sense of action over the orbit starting from the point $p=0$, $x=1/2^k$.

7. On distribution and degeneracy of eigenvalues of quantum Arnold's cat map for inverse Planck's constant $N=4^k$

In Fig. 2 a box is drawn at each vertex of the graph, which contains coordinates (p,x) of a starting point and a value of action S_T for the corresponding periodic orbit. At zero level of the graph we have the fixed point (0, 0) and zero value of action. According to Eq. (15), it gives a single eigenvector with eigenvalue $\lambda=1$. At the level $k=1$ we have one period-3 cycle with zero action. It gives three eigenvectors with eigenvalues 1, $\mathrm{e}^{2\pi\mathrm{i}/3}$, $\mathrm{e}^{-2\pi\mathrm{i}/3}$. For next levels of the graph the actions are $S_T=(2j+1)/M$, $j=0,1,\ldots,(M/2)-1$, where $M=2^k$, $k\geq 2$, and the orbits are of period $T=\frac{3}{4}M$. According to Eq. (15), such an orbit gives rise to T eigenvectors characterized by a set of eigenvalues $\lambda_s=\exp[2\pi\mathrm{i}(S_T+s)t/T]$, $s=0,1,\ldots,T-1$.

For $M=2^k>1$ and any given $S=(2j+1)/M$ one can find two orbits possessing such a value of action. It follows from solution of Eq. (26) regarded as a quadratic congruence (see e.g. [42]). So, each number S occurs twice, once in the left half of the graph, and once in the right half. It means that the eigenvalues are twice degenerated.

We conclude that in the discussed case the distribution of eigenvalues of the quantum Arnold's cat map on the unit circle is rather simple, regular, and has nothing common with predictions of the random matrix theory [1–12,43,44]. Namely, for a given N the eigenvalues are located at the angles $\theta=2\pi n/T_{\mathrm{H}}=8\pi n/3N$, where n is either an odd integer or an odd number multiplied by a power of 4. Except two singlets ($\pm 2\pi/3$), all the eigenvalues are twice degenerated. As an example, Fig. 4 shows spectrum of our quantum system for a particular case $M=8$, $N=64$ and explains correspondence of quantum eigenstates and classic orbits. Points of each orbit on the lattice 8×8 (diagram (a)) are marked with the same symbol as the vertices of the graph (b) and as the associated eigenvalues on the unit circle (c).

8. Quantum evolution of localized Gaussian wave packet: spectral properties of quantum chaos in connection with Wiener–Khinchin theory

Let us consider Gaussian wave packet of minimal uncertainty, with zero mean coordinate and momentum, as an initial state of the quantum system. Accounting periodicity condition for wave function in the position representation, we supplement the main packet by its multiple copies shifted by integer numbers of periods. Thus, we set

$$\Psi_m^0=C(N)\sum_{\chi=-\infty}^{\infty}\mathrm{e}^{-\pi(m-\chi N)^2/N},\quad m=0,1,2,\ldots,N-1. \tag{30}$$

In the case of interest, $N\gg 1$, the normalizing factor $C(N)$ may be equated to $\sqrt[4]{2/N}$. The Gelfand transform of this state vector may be found from Eq. (6) and written as

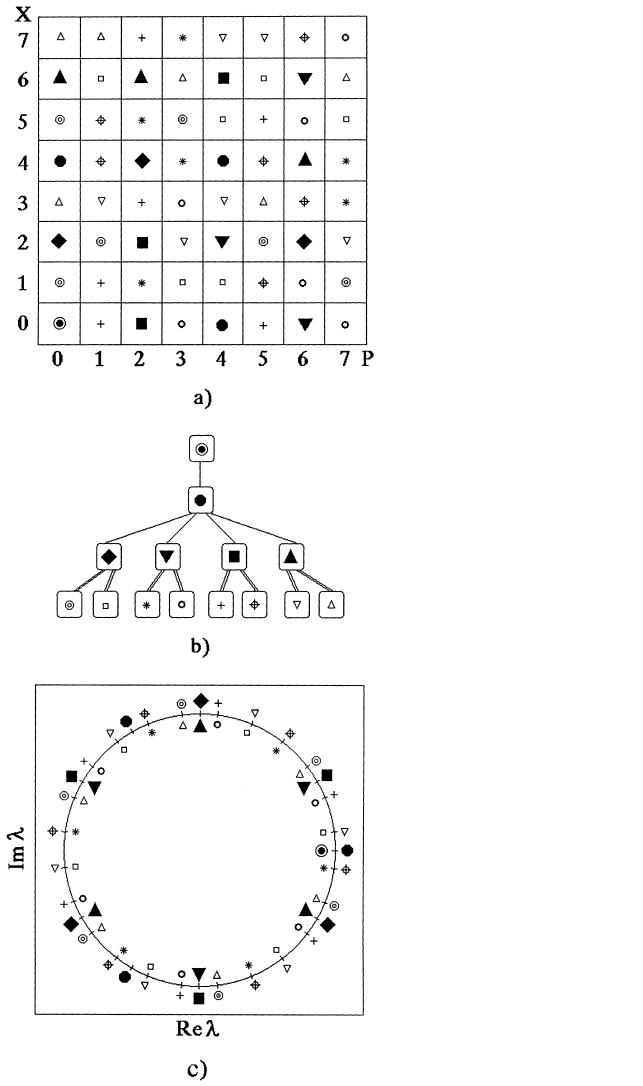

Fig. 4. Periodic orbits of classic Arnold's cat map and their connection with spectrum of the quantum evolution operator for $N = M^2 = 64$. (a) Sites on the lattice $M \times M$ which belong to different periodic orbits; points of each orbit are marked by a definite symbol. (b) Tree-like graph explaining the ordering of the periodic orbits. Edges shown by single lines mean preservation of a period, while doubled lines correspond to period doubling. (c) Eigenvalues of the evolution operator localized on the unit circle. The same symbols as in diagrams (a) and (b) mark eigenvalues generated by the respective cycles of the classic map (13). Note that all eigenvalues, with exception of two, are twofold degenerated.

$$w_{ml} = \frac{\sqrt[4]{2}}{M} W(m/M, l/M), \quad W(\xi, \eta) = \sum_{\chi=-\infty}^{\infty} \mathrm{e}^{-\pi(\xi+\chi)^2 + (2\pi \mathrm{i} m/M)(\eta+\chi)}. \tag{31}$$

Formally, this expression includes an infinite sum. However, the convergence is very fast, so it is sufficient to account only three or five terms with $\chi = 0, \pm 1, \pm 2$ to represent w_{ml} with high precision. Now, as follows from Eq. (20),

$$C^{(\mu,r)} = \frac{\sqrt[4]{2}}{M\sqrt{T}} \sum_{t=0}^{T-1} \sum_{\chi=-\infty}^{\infty} W(m/M, l/M)\, \mathrm{e}^{-2\pi \mathrm{i} S_t + (2\pi \mathrm{i}/T)(S_T + r)t}. \tag{32}$$

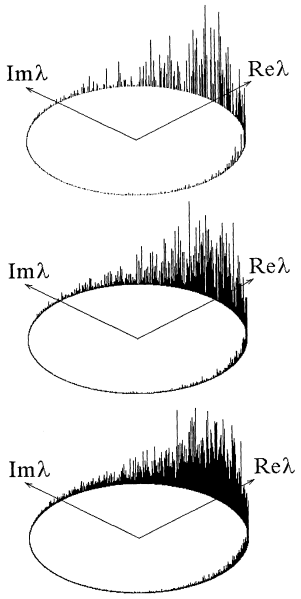

Fig. 5. Spectral intensity distribution over eigenvalues of the quantum Arnold's cat map for Gaussian wave packet of minimal uncertainty with zero mean coordinate and momentum. From up to down: $M = 32, 64, 128$, and $N = 1024, 4096, 16\,384$, respectively. Vertical segments are drawn from those points of the unit circle which belong to the spectrum of eigenvalues of the evolution operator. Length of each segment means a sum of squared absolute values of coefficients at eigenvectors associated with the given eigenvalue.

According to foundations of quantum mechanics, squared modulus of a coefficient $C^{(\mu,r)}$ is a probability for the system to be found in the eigenstate of the evolution operator. This probability may be thought as a measure concentrated at that point of unit circle where the eigenvalue is located. As it has been mentioned, in the case of our interest almost all eigenvalues are twice degenerated. So, the measure attributed to the corresponding points of the unit circle is a sum of two terms representing probabilities of two eigenstates, $I_i = \left|C^{(\mu_1,s_1)}\right|^2 + \left|C^{(\mu_2,s_2)}\right|^2$. Of course, the spectral intensity distribution $\{I_i\}$ will depend on the form of the analyzed wave packet. For our case of Gaussian wave packet (30) the plot of the distribution is shown in Fig. 5. It looks like a sample spectrum of a stationary random process called 'periodogram'. In particular, variance of the amplitude is of order of the amplitude itself. Analogous spectral intensity distributions for quantum systems are considered in context of theory of scars [45,46].

Let us turn to a subset of coefficients, which are associated with a given orbit of period T. With respect to index r, these coefficients have period T. Hence, we can apply Fourier transformation to squared moduli of the coefficients and obtain a function

$$\begin{aligned}\kappa_\mu(\tau) &= \sum_{r=0}^{T-1} \left|C_r^{(\mu,r)}\right|^2 \mathrm{e}^{-(2\pi\mathrm{i}/T)\tau r} = \sum_{t=0}^{T-1} w_{m_{t+\tau},l_{t+\tau}} w^*_{m_t,l_t}\, \mathrm{e}^{-2\pi\mathrm{i}(S_{t+\tau}-S_t)+(2\pi\mathrm{i}/T)S_T\tau} \\ &= \frac{\sqrt{2}}{M^2}\mathrm{e}^{(2\pi\mathrm{i}/T)S_T\tau} \sum_{t=0}^{T-1} W\left(\frac{m_{t+\tau}}{M}, \frac{l_{t+\tau}}{M}\right) W^*\left(\frac{m_t}{M}, \frac{l_t}{M}\right) \\ &\quad \times \exp\left(-\frac{2\pi\mathrm{i}}{M^2}\sum_{j=t}^{t+\tau-1}\left(\frac{m_{j+1}^2}{2} - m_{j+1}m_j + m_j^2\right) + \frac{\pi\mathrm{i}\tau}{4}\right). \end{aligned} \tag{33}$$

This is a kind of correlation function. It characterizes correlations in the complex sequence $w_t = W(m_t/M, l_t/M)\exp(-2\pi\mathrm{i}(S_t - S_T t/T))$, which is generated when m_t and l_t run over the periodic orbit on the lattice $M \times M$. Summation in Eq. (33) may be interpreted as time averaging of some dynamical function $F_\tau(m_t/M, l_t/M)$ over a period of the cycle. In fact, to obtain $\kappa_\mu(\tau)$ we must deal rather with a family of these dynamical functions, which depend on an integer parameter τ, namely

$$F_\tau(\xi,\eta) = \sqrt{2}W(\xi_\tau,\eta_\tau)W^*(\xi,\eta)\exp\left(-2\pi\mathrm{i}\sum_{j=0}^{\tau-1}\left(\frac{\xi_{j+1}^2}{2} - \xi_{j+1}\xi_j + \xi_j^2\right) + \frac{\pi\tau}{4}\right), \tag{34}$$

where ξ_τ and η_τ are to be found from

$$\xi_{t+1} = \eta_t + 2\xi_t, \quad \eta_{t+1} = \eta_t + \xi_t + 1/2 \pmod 1, \tag{35}$$

$$\xi\,|_{t=0} = \xi, \quad \eta|_{t=0} = \eta. \tag{36}$$

It is convenient to redefine normalization as

$$K_\mu(\tau) = \frac{M^2}{T}\kappa_\mu(\tau) = \mathrm{e}^{(2\pi\mathrm{i}/T)S_T\tau}\overline{F_\tau(m_t/M, l_t/M)}, \tag{37}$$

where overline designates the time average.

Let us build a construction analogous to Eq. (37), but with change of the time average to the average over the natural measure of the classic map (35). This map is reduced to the Arnold's cat map (2) by a shift of origin. Hence, the invariant measure is the uniform distribution on the unit square $0 \le m/M < 1$, $0 \le l/M < 1$ [15], and we set

$$K(\tau) = \langle F_\tau(\xi,\eta)\rangle = \int_0^1\int_0^1 F_\tau(\xi,\eta)\,\mathrm{d}\xi\,\mathrm{d}\eta. \tag{38}$$

The classic map is mixing, so for $\tau \to \infty$ correlation disappears, and $K(\tau) \to 0$.

It is worth discussing behavior of the correlation functions $K_\mu(\tau)$ and $K(\tau)$ in more details. Suppose we look over the periodic orbits of the classic map, going down from level to level of the tree-like graph of Fig. 2. How do $K_\mu(\tau)$ and $K(\tau)$ relate at very deep levels?

At a definite level of number k we have $M = 2^k$ and $T = \frac{3}{4}M$. Due to chaotic dynamics of the classic map, orbits of long periods look like sets of points randomly scattered over sites of the lattice $M \times M$. In fact, their distribution corresponds to the invariant measure, this assertion is known as Bowen theorem [47,48]. Hence, roughly speaking, $K_\mu(\tau)$ may be regarded as a result of evaluation of the integral in Eq. (38) by Monte-Carlo method [49], but instead of randomly scattered points in the integration area (the unit square), the points are taken which belong to one orbit of the classic chaotic map.[2] It is known that the error of the Monte-Carlo calculation is proportional to inverse square root of number of points, so $\left|K_\mu(\tau) - K(\tau)\right| = 1/\sqrt{T}$. Thus for $k \to \infty$, $K_\mu(\tau)$ approaches $K(\tau)$. In other words, $K(\tau)$ may be interpreted as classic limit of function $K_\mu(\tau)$. As we mentioned, for large τ $K(\tau) \to 0$. So, in this region $K_\mu(\tau)$ has fluctuations of order $\left|K_\mu(\tau)\right| \cong 1/\sqrt{T} \cong 1/\sqrt{M}$.

Now it is useful to appeal to analogy with spectral-correlation theory of stationary random processes [50]. $K(\tau)$ corresponds to convenient correlation function of a random process, while $K_\mu(\tau)$ is analogous to a sample correlation function estimated over a finite-time individual realization of the process. Fourier transform of $K(\tau)$ corresponds to Wiener–Khinchin spectral density. In turn, from a sample correlation function one obtains a spectral distribution known as periodogram — an estimate of spectral density which is not consistent (statistical fluctuations are of the same order as the estimated variable). In our quantum problem Fourier transformation of $K_\mu(\tau)$ returns us to the

[2] Considering passage to the limit $k \to \infty$ for a fixed τ we may ignore the factor $\exp(2\pi\mathrm{i}S_T\tau/T)$ in Eq. (37) because it tends to unity.

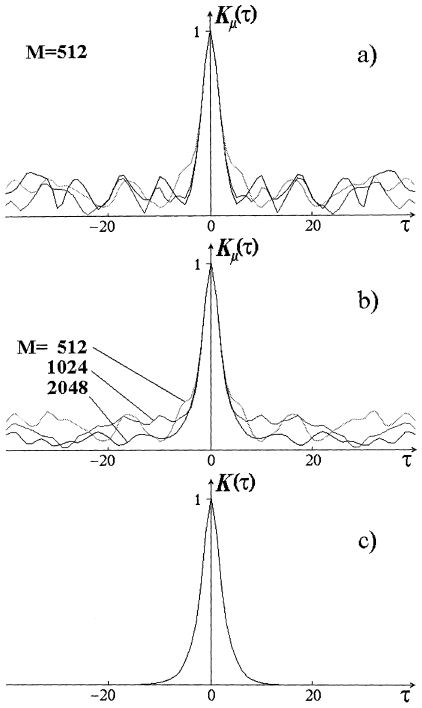

Fig. 6. Correlation functions obtained by time averaging over a period for certain cycles ((a) and (b)), and by averaging over the invariant measure (c). Correlation functions calculated for cycles of the same period $T = 384$ demonstrate fluctuations of the same order at large t (a). (b) gives evidence that the magnitude of the fluctuations decreases with growth of T (in fact, as $1/T^{1/2}$). Comparison of (a) and (b) with (c) shows that configuration of the main peak is formed due to averaging over the invariant measure. The initial state of the system is the Gaussian wave packet of minimal uncertainty with zero mean coordinate and momentum.

probability measure discussed after formula (32). So, this distribution is just the counterpart of the periodogram. According to the analogy with the Wiener–Khinchin theory, Fourier transform for $K(\tau)$:

$$S(\theta) = \sum_{\tau=-\infty}^{\infty} K(\tau)\, \mathrm{e}^{-\mathrm{i}\theta\tau} \tag{39}$$

is the smoothed density of the above probability measure. As usually, it means that $S(\theta)\Delta\theta$ is the probability for the system to be found in a state with eigenvalue $\exp(\mathrm{i}\theta)$ with θ hitting into the interval of width $\Delta\theta$. The function $S(\theta)$ is a well-defined characteristic of the probability measure, like Wiener–Khinchin spectral density is in the theory of random processes.

Let us illustrate the above discussion numerically

In Fig. 6(a) correlation functions $K_\mu(\tau)$ are shown, which are computed for $M = 512$ by means of time averaging over three different cycles of period 384. It may be seen that at large t all three curves show fluctuations of the same order of magnitude. In Fig. 6(b) we compare the functions $K_\mu(\tau)$ for cycles related to different levels of the graph. The values of M are 512, 1024, 2048, and respective periods are equal to $\frac{3}{4}M$. The plot demonstrates that intensity of the fluctuations decreases with growth of the level number (in fact, as $2^{-k/2} \cong 1/\sqrt{T} \cong 1/\sqrt{M}$).

The function $K(\tau)$ was computed by averaging over the invariant measure of the classic map, i.e. by means of numerical integration of Eq. (38) on square net $2^k \times 2^k$ with control of precision by increase of k (see Table 1). Fig. 6(c) shows a plot of $K(\tau)$. Comparison of Fig. 6(a) and (b) with (c) gives evidence that formation of the main peak of the correlation function is associated with averaging over the invariant measure.

Table 1
Function $K(\tau)$ obtained by numerical integration

τ	$K(\tau)$
0	1.0000000
1	0.8164966
2	0.5345525
3	0.3333333
4	0.2062843
5	0.1275154
6	0.0788110
7	0.0487081
8	0.0301033
9	0.0186049
10	0.0114984
11	0.0071064

It may be seen that for large τ the function $K(\tau)$ behaves as const.$\cdot \mathrm{e}^{-\Lambda|\tau|/2}$, where $\Lambda = \log[(3+\sqrt{5})/2]$ is the Lyapunov exponent. So, as expected, characteristic time of decay of correlation is of order of $1/\Lambda$. Moreover, the data are fitted well by the ansatz

$$K(\tau) = 1/\sqrt{\cosh(\Lambda\tau)} \tag{40}$$

known as a result of linear analysis of semiclassic evolution near unstable fixed points and used in the theory of scars [46].

In Fig. 7 the spectral density

$$S(\theta) = 1 + 2\sum_{\tau=1}^{\infty} \frac{\cos\theta\tau}{\sqrt{\mathrm{coshrm}(\Lambda)\tau}} \tag{41}$$

and true distribution of the probability measure over the unit circle are compared.

Now instead of the wave packet centered at the origin let us consider packets with center shifted with respect to spatial coordinate and/or momentum. Let the shifts be defined by values Δp and Δx, and normalized in such a way that unity corresponds to a period on the torus. State vector of such a packet in usual position representation is constructed by modification of expression (30) as follows:

$$\psi_m^{(\Delta p,\Delta x)} = \sqrt[4]{\frac{2}{N}} \sum_{\chi=-\infty}^{\infty} \mathrm{e}^{-(\pi(m-[N\Delta x]-\chi N)^2/N)+(2\pi \mathrm{i}/N)m[N\Delta p]}, \quad m = 0, 1, 2, \ldots, N-1. \tag{42}$$

During the passage to the classic limit $N\to\infty$ the values Δp and Δx should be kept constant. If one of these shifts is non-zero, Gelfand's transform w_{ml} does not tend to a smooth function of the arguments m/M and l/M, as for the packet (30), but has oscillations on a scale $1/M$.

Suppose we select Δp and Δx by chance, and consider a property which takes place with probability close to 1. Such a situation may be referred to as 'generic'. Averaging over the invariant measure (38) for generic wave packet yields small values even for small τ, i.e. the correlation function does not have the main maximum. On the other hand, the Monte-Carlo argumentation holds, so the correlation functions remain to be random-like with oscillations of order of magnitude $1/\sqrt{M}$. The spectral intensities are represented by a random-like set of amplitudes with fluctuations of order of the amplitudes themselves. In this case there are not any spectral regions of greater or lesser mean intensity. The probability measure looks like a statistically uniform distribution of the amplitudes over the entire set of the eigenvalues.

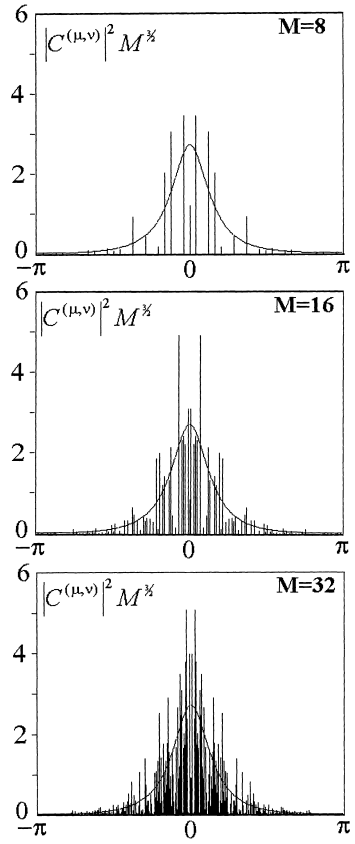

Fig. 7. Spectral intensity distribution (as in Fig. 5) in comparison with spectral density defined by analogy with Wiener–Khinchin theory for $M = 8$, 16, 32. The initial state of the system is the Gaussian wave packet of minimal uncertainty with zero mean coordinate and momentum.

In Fig. 8 we compare spectral intensity distributions for wave packets with $\Delta p = 0$, 0.5, 0.25, 0.125, and for a packet selected as a 'generic example', with $\Delta p = 0.171398736$. (For all the packets we take the coordinate shift Δx to be zero.)

If there are some localized spectral regions of relatively greater mean intensity, it may be interpreted as presence of scarring. This is a property of a representative set of eigenstates to have anomalous enhancement of amplitudes near unstable classical short-period orbits [45,46]. Such eigenstates obviously bring greater contribution to the probability measure if the wave packet is centered at points of the mentioned orbits. In this sense, Fig. 8(a) illustrates scarring associated with the fixed point of the classic map at the origin, while Fig. 8(b)–(d) illustrate scarring corresponding to orbits of period 3 and 6. (Note that here we speak about periodic orbits of the classic map (2), which should not be confused with orbits on the lattice $M \times M$ discussed in connection with dynamics in Gelfand's representation.)

We conclude that in all cases the spectral intensity distributions over eigenstates of the quantum Arnold's cat map for originally localized wave packets have the following properties. First, a majority of components have amplitudes of comparable order, such a spectrum may be called dense. [3] Second, the intensity distribution has local random-like

[3] Alternatively, we could speak about a sparse spectrum when relatively small number of eigenstates yields major contribution to the probability measure. Such situation is typical for regular dynamics. The regular dynamics sometimes may yield also a dense spectrum, but it does not manifest the random-like local structure.

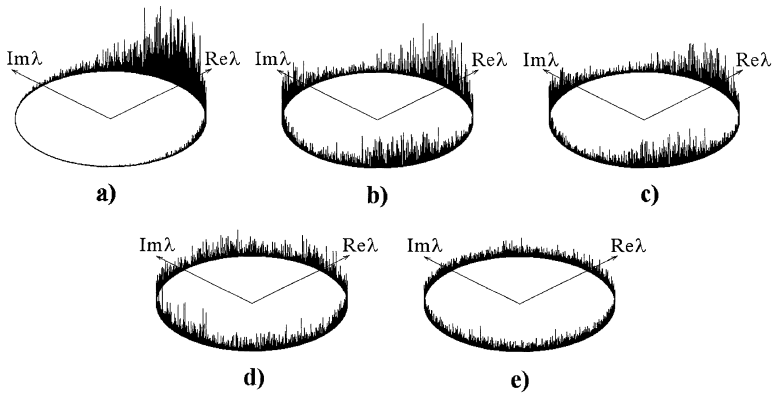

Fig. 8. Spectral intensity distributions for Gaussian wave packets of minimal uncertainty. Shifts from the origin for the packets are (a) $\Delta p = 0$, (b) $\Delta p = 0.5$, (c) $\Delta p = 0.25$, (d) $\Delta p = 0.125$, (e) $\Delta p = 0.171398736$ (generic wave packet).

structure, it means that in any small spectral interval the amplitudes of eigenstates are scattered randomly, and may be thought, at least in good approximation, as statistically independent. (In the presence of scarring a mean level of amplitudes and their fluctuations may manifest smooth variations and be essentially different in different spectral intervals.) We have seen that for quantum Arnold's cat map such a character of spectra, similar to a sample spectrum of a random process, is linked closely with chaotic behavior of the classic map.

9. Statistics of spectral intensity distributions at quantum chaos

Chaos in classic dynamics is associated with continuous spectrum while regular periodic or quasi-periodic motion with discrete spectrum. Spectral intensity distributions generated by quantum Arnold's cat map, although discrete, have a combination of properties intrinsic to sample spectra of random processes. In this section we discuss several statistics aimed to reveal these properties, and hence, to distinguish quantum chaos and regular dynamics.

The first test consists in plotting diagrams, which give clear visual evidence that spectrum is dense and has local random-like structure. Let us take a sequence of intensities $\{I_i\}$ and subdivide it into a set of triplets (I_{n-1}, I_n, I_{n+1}). Then, in three-dimensional space (x, y, z) the points

$$x = I_{n-1}/(I_{n-1} + I_n + I_{n+1}), \quad y = I_n/(I_{n-1} + I_n + I_{n+1}), \quad z = I_{n+1}/(I_{n-1} + I_n + I_{n+1}) \tag{43}$$

fall onto a plane $x+y+z = 1$ inside an equilateral triangle. For spectral intensity distributions generated by the quantum Arnold's cat map we can see that the points fill interior of the triangle in a random manner (Fig. 9).

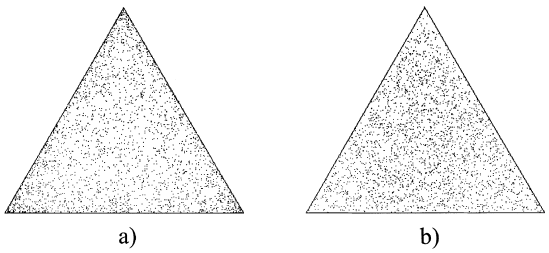

Fig. 9. Visual test of randomness of local structure of the intensity spectrum (see text). Statistically uniform scattering of points over interior of the equilateral triangle implies presence of local random structure of the spectrum. Diagram (a) relates to a wave packet centered at the origin, diagram (b) to a wave packet with shift $\Delta p = 0.171398736$. Quantum parameter (inverse Planck's constant) is $N = 2^{14}$.

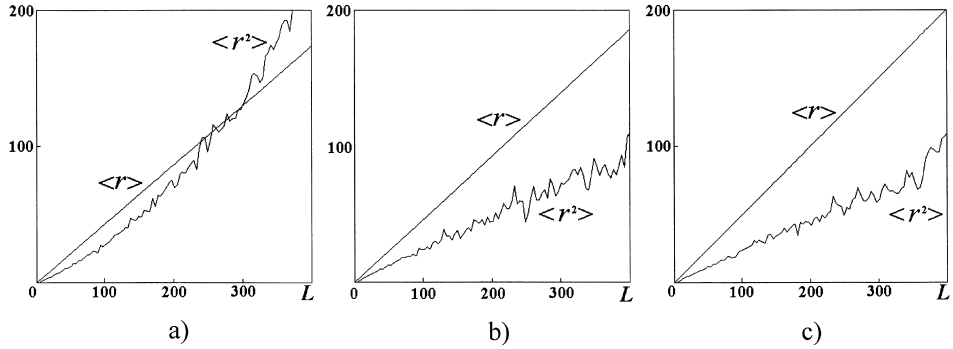

Fig. 10. Comparison of tests for statistical independence of spectral intensities for (a) wave packet centered at the origin, (b) wave packet with shift $\Delta p = 0.171398736$, and (c) surrogate random sequence. Quantum parameter (inverse Planck's constant) is $N = 2^{18}$. The plots show mean value and variance of number of groups in samples versus the volume of samples (see text).

Apparently, it implies statistical independence of neighbor terms and random scattering intrinsic to the processed sequence $\{I_i\}$.

The second test is aimed to a quantitative verification of statistical independence of the spectral intensities, it is some version of a procedure known in mathematical statistics [50]. Let us take a spectral interval containing L eigenvalues, and the intensities are $I_1, I_2, \ldots, I_L$. We define r as a number of groups formed by neighbor terms of the sequence I_i, which are all greater, or all less, than the mean value $\bar{I} = (1/L)\sum_{i=1}^{L} I_i$. (Say, a sequence of signs $+,+,+,-,-,+,-,-,-,+,+,-,-$ contains $r = 6$ groups.) For a fixed L we can select different spectral intervals and calculate mean $\langle r \rangle$ and variance $\langle \Delta r^2 \rangle$. Then we can study dependence of these values on L. It may be proven that this procedure applied to a real random sequence for large L yields $\langle r \rangle \cong L/2$ and $\langle \Delta r^2 \rangle \cong L/4$. Similar statistics are manifested by the cat map spectral distributions for generic wave packets, although the growth is a little bit slower (Fig. 10). For wave packet centered at the origin the behavior characteristic for a random sequence is observed only for small L. For larger L deflections appear which imply presence of distant correlations. Apparently, it is connected with presence of slow spectral envelope and scarring.

The third test analyzes local statistical properties of the spectral intensity distributions. We again divide the sequence $\{I_i\}$ into groups of L terms and construct histogram counting numbers of terms in each interval $k\Delta I \leq I < (k+1)\Delta I$, where $\Delta I = \text{const}$. This is an estimate of the probability density function. From the same data one can also calculate a cumulative distribution function. In Fig. 11 the results are shown for the case of the wave packet centered at the origin and in Fig. 12 for a generic wave packet. They appear to be close to chi-squared distributions with one and two degrees of freedom, respectively.[4] It may be seen from comparison of the empirical data with a theoretical distribution (solid curve) and with results of processing of a surrogate random sequence of the same volume. So, the local spectral distributions are consistent, at least roughly, with those predicted by random matrix theory (spectrum of Porter–Thomas) [10,43,46], although in case (a) statistically significant deflections from the theoretical distribution are present in spectral intervals of lower mean intensity. This observation seems interesting and significant because in other aspects (say, concerning eigenvalue distribution) our map does not demonstrate any correspondence with the random matrix theory.

[4] Reason for appearance of the chi-squared distribution of two degrees of freedom is that almost all eigenstates are twice degenerated, while intensities related to one eigenvalue are summarized. The case of the packet centered at the origin is exceptional. Due to symmetry, it appears that amplitudes of any pair of the degenerate states are exactly equal. So, presence of degeneracy does not affect the structure of the probability distribution, and it is close to chi-squared of one degree of freedom.

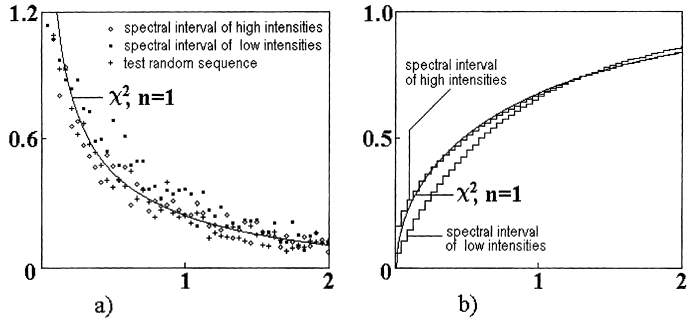

Fig. 11. Comparison of statistical estimates of the probability density function and cumulative distribution function for Gaussian wave packet centered at the origin with chi-squared distribution of one degree of freedom (solid curve). Quantum parameter is $N = 2^{18}$. Two spectral intervals were processed, each contained 4096 eigenvalues. One was taken in the region of high intensities (diamonds) and another in the region of low intensities (squares). Crosses correspond to data for surrogate random sequence of the same volume obeying the chi-squared distribution of one degree of freedom. Note statistically significant deflection from χ^2-distribution observed in spectral region of low amplitudes.

The last test is aimed to distinguish the situations of dense and sparse spectra by calculation of the inverse participation ratio (IPR) [46]. Let us divide the interval of eigenangles $[-\pi, \pi]$ into subintervals of equal width $\Delta\theta$. By averaging over all I_i inside each interval we find the corresponding local values of IPR, namely,

$$\mathrm{IPR} = L_{\Delta\theta}\langle I_i^2\rangle / \langle I_i\rangle^2 , \tag{44}$$

where $L_{\Delta\theta}$ stands for a number of eigenvalues in the spectral interval $\Delta\theta$. For a dense spectrum majority of values I_i are of the same order, and IPR is of order unity. For opposite limit case, when only a few of intensities in the group are notably distinct from zero, we would have IPR of order $L_{\Delta\theta}$. Processing of the intensity spectra for the quantum Arnold's cat map shows that they are dense (Fig. 13). Local values of IPR correspond, although roughly, to those expected for the chi-squared distributions: for wave packet centered at the origin IPR oscillates near 3, while for a generic packet near 2.

As known [46], global IPR, obtained by averaging over an entire spectrum is effective tool for analysis of scarring. In Fig. 14 we plot this value versus the inverse Planck's constant N. It may be seen that for the packet centered at the origin the value of IPR grows linearly in dependence on $\log N$. Analogous, although slower growth, is observed for

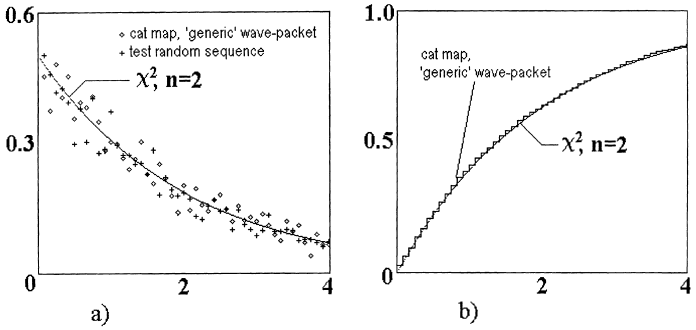

Fig. 12. Comparison of statistical estimates of the probability density function and cumulative distribution function for Gaussian wave packet shifted from the origin ($\Delta p = 0.171398736$) with chi-squared distribution of two degrees of freedom (solid curve). Quantum parameter is $N = 2^{18}$. The processed spectral interval contained 4096 eigenvalues (diamonds). Crosses correspond to data for surrogate random sequence of the same volume obeying the chi-squared distribution of two degrees of freedom.

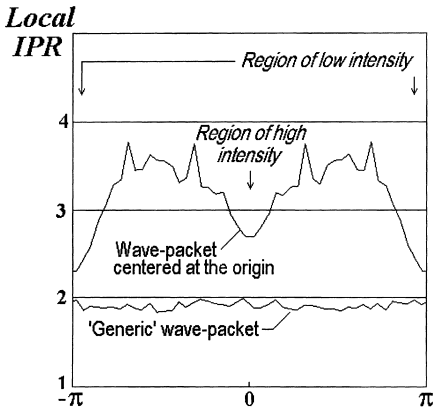

Fig. 13. Local inverse participation ratio found for eigenangle intervals from $\theta - \Delta\theta/2$ to $\theta + \Delta\theta/2$, where $\Delta\theta = \pi/24$, for a wave packet centered at the origin and for a shifted wave packet ($\Delta p = 0.171398736$). Quantum parameter is $N = 2^{18}$.

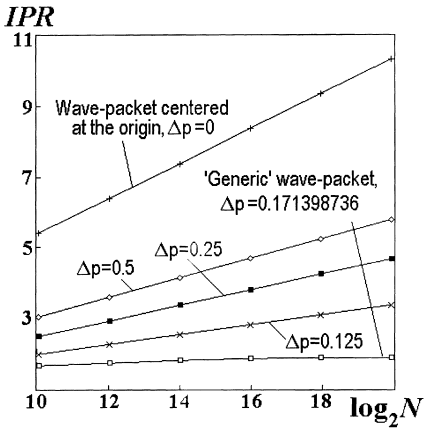

Fig. 14. Inverse participation ratio found for entire spectral intensity distribution versus the quantum parameter N (the inverse Planck's constant). The data are presented for wave packets centered at the origin ($\Delta p = 0$), at classic orbits of period 3 ($\Delta p = 0.5$ and 0.25), of period 6 ($\Delta p = 0.125$), and for 'generic' packet with an arbitrarily chosen Δp.

packets with $\Delta p = 1/2$, 1/4, 1/8. For sufficiently large N the value of IPR becomes greater than 3. It gives evidence of scarring which is associated for $\Delta p = 0$ with a fixed point of the classic map, and for $\Delta p = 1/2$, 1/4, 1/8 with its unstable orbits of period 3 and 6. Increase of IPR in dependence on N means that degree of scarring grows in the process of passage to the classic limit. (Perhaps, this is a peculiarity of our model, which may be not intrinsic to other systems with quantum chaos.) For generic wave packet IPR does not show a tendency to grow and remains close to 2. Hence, there is no scarring in this case.

10. Conclusion

As known, a basic problem of quantum chaology consists in investigation of details of quantum–classic correspondence. In the present paper passage to the classic limit in the quantum Arnold's cat map is considered for a

situation when the inverse Planck's constant increases according to a power law $N=4^k$. It may be thought that similar approach may be productive for other quantum systems. Because of the enforced regularity of the quantum parameter increase, passage to the limit accepts some regularity too; further complicated and non-trivial details may be postponed to next stages of the research. One could compare this approach with renormalization group analysis, proved to be an effective tool for study of the onset of chaos in classic nonlinear dynamics. Ultimately, discussing passage from quantum to classic domain we also deal with a kind of scenario of transition to chaos.

In the case under consideration the quantum parameter is a perfect square, $N=M^2$. It gives an opportunity to use a representation based on a discrete version of Gelfand's transformation, which leads to a picture of dynamics remarkably close to that adopted in old quantum mechanics. Namely, we come to dynamics on a lattice of size $M\times M$ governed by the classic Arnold's cat map and supplemented by evolution of a phase variable, which is proportional to the classic action.

Being given some initial wave function, in Gelfand's representation we have some distribution of complex amplitudes on a set of sites of the lattice $M\times M$. Each periodic orbit on this lattice generates then a sequence of the complex amplitudes, and this sequence may be processed by means of discrete Fourier transformation. It yields a set of coefficients for expansion of the wave function over eigenstates of the evolution operator. The full set of the coefficients is obtained when we account all periodic orbits on the lattice $M\times M$.

Due to chaotic nature of the classic map, its long-period orbits consist of points scattered over the lattice in a random manner. Hence, a sequence of complex amplitudes generated by such an orbit and its Fourier transform are random-like too. It follows then that majority of spectral amplitudes is of comparable order of magnitude, and random variance of the amplitudes is of the same order as the amplitudes themselves. In the presence of scarring, when the spectral intensity distribution has a smooth envelope, the above properties have to be understood as local, relating to spectral intervals narrow in comparison to the scale of the smoothed spectrum, but large in comparison with the inverse Heisenberg time. Appealing to analogy with Wiener–Khinchin theory of random processes, one can say that the spectral intensity distribution over the eigenstates is similar to a spectrum of individual sample of a random process (periodogram). Smoothed intensity distribution appears as analog of Wiener–Khinchin spectral density, and this is a characteristic possessing well-defined classic limit. In other words, relation between quantum and classic chaos is similar to that between a finite-time sample of a random process and the process itself.

Acknowledgements

This work was supported by Russian Foundation of Fundamental Researches (grant 97-02-16414).

Appendix A. Explicit evaluation of factor R — the action for fundamental orbit

As we mentioned in the main text, action for orbits of period $T=\frac{3}{4}M$ for $M=2^k$ may be calculated from Eq. (25). It contains a factor R defined as action for the fundamental orbit:

$$R=S_T^0=\frac{1}{M^2}\sum_{t=0}^{T_0-1}(X_{t+1}^2/2-X_{t+1}X_t+X_t^2-X_tM/2),\quad X_0=1,\ P_0=0. \tag{A.1}$$

Here we derive an explicit expression for this factor for $k\geq 3$, i.e. $M\geq 8$.

Excluding momentum P, one can rewrite map (13) as one difference equation of the second order

$$X_{m+1}-3X_m+X_{m-1}=0 \pmod M. \tag{A.2}$$

Initial conditions for the fundamental orbit are

$$X_0 = 1, \quad X_{-1} = 1, \tag{A.3}$$

and from the property of symmetry of Eq. (A.2) we conclude that

$$X_t = X_{T-t-1} \pmod{M}. \tag{A.4}$$

Let us transform Eq. (A.1) taking into account that only the fractional part of R is relevant. The last term in Eq. (A.1) vanishes after summation modulo M. Indeed, summation over the complete cycle in Eq. (13) yields $\sum_{t=0}^{T-1} X_t = 0$. Further, due to the symmetry $X_t = X_{T-t-1}$ and evenness of period T ($k \geq 3$), we have $\frac{1}{2}\sum_{t=0}^{T-1} X_t = 0 \pmod{M}$. Due to cyclicity with respect to t and symmetry property (A.4), we rewrite Eq. (A.1) as

$$R = \left\{ \sum_{t=0}^{T/2-1} \left(\frac{X_t}{M}\right)\left(\frac{X_{t+1} + 3X_t - X_{t-1}}{M}\right) \right\}, \tag{A.5}$$

where braces mean the fractional part.

Beside X, it is convenient to use an integer variable Q governed by Eq. (A.2), but without taking modulus,

$$Q_{m+1} - 3Q_m + Q_{m-1} = 0, \tag{A.6}$$

with initial conditions

$$Q_0 = 1, \quad Q_1 = 1. \tag{A.7}$$

Obviously, Q_t are Fibonacci numbers, $Q_t = F_{2t+1}$, where $F_0 = 0, F_1 = 1, F_2 = 1, F_3 = 2, \ldots, F_{t+1} = F_t + F_{t-1}$.

Note that the second co-factor in Eq. (A.5) is an integer by Eq. (A.2). Hence, the value of R remains the same after a change of X_t/M to Q_t/M. So, we have

$$\begin{aligned}
R &= \left\{ \sum_{t=0}^{T/2-1} \left(\frac{Q_t}{M}\right)\left(\frac{X_{t+1} + 3X_t - X_{t-1}}{M}\right) \right\} = \left\{ \sum_{t=0}^{T/2-1} \frac{Q_t}{M}\frac{3X_t}{M} - \sum_{t=0}^{T/2-1} \frac{Q_t}{M}\frac{X_{t+1}}{M} - \sum_{t=0}^{T/2-1} \frac{Q_t}{M}\frac{X_{t-1}}{M} \right\} \\
&= \left\{ \sum_{t=0}^{T/2-1} \frac{3Q_t}{M}\frac{X_t}{M} + \frac{Q_{-1}X_0}{M^2} - \sum_{t=0}^{T/2-1} \frac{Q_{t-1}}{M}\frac{X_t}{M} - \frac{Q_{T/2-1}X_{T/2}}{M^2} \right. \\
&\quad \left. - \frac{Q_0 X_{-1}}{M^2} - \sum_{t=0}^{T/2-1} \frac{Q_{t+1}}{M}\frac{X_t}{M} + \frac{Q_{T/2}X_{T/2-1}}{M^2} \right\} \\
&= \left\{ \frac{Q_{T/2}X_{T/2-1} - Q_{T/2-1}X_{T/2}}{M^2} + \sum_{t=0}^{T/2-1} \left(\frac{-Q_{t+1} + 3Q_t - Q_{t-1}}{M}\right)\left(\frac{X_t}{M}\right) \right\}.
\end{aligned}$$

The term under summation symbol vanishes according to Eq. (A.6). Finally, we note that $Q_{T/2-1} = F_{T-1}$, $Q_{T/2} = F_{T+1}$, and as may be shown, $X_{T/2} = X_{T/2-1} = (M/2)+1$. So,

$$R = \left\{ \frac{(M/2)+1}{M^2}(F_{T+1} - F_{T-1}) \right\} = \left\{ \frac{(M/2)+1}{M^2} F_T \right\}. \tag{A.8}$$

The required Fibonacci numbers with indices $T = 3\cdot 2^{k-2}$ may be computed recursively via the relations

$$y' = 2yz - y^2, \quad z' = y^2 + z^2. \tag{A.9}$$

Starting from $i=0$, $k=3$, and $(y, z)=(F_6, F_7)=(8, 13)$, after n iterations of Eq. (A.9) one obtains $(y,\ z) = (F_{3\cdot 2^{n+1}},\ F_{3\cdot 2^{n+1}+1})$.

References

[1] P. Cvitanovic, I. Percival, A. Wirzba (Eds.), Quantum Chaos — Quantum Measurement, Kluwer Academic Publishers, Dordrecht, 1992.
[2] G.M.Zaslavsky. Stochasticity of Dynamical Systems (Stokhastichnost' Dinamicheskikh Sistem), Nauka, Moscow, 1984.
[3] B. Eckhardt, Phys. Rep. 163 (1988) 205.
[4] K. Nakamura, Quantum Chaos. A New Paradigm of Nonlinear Dynamics, Cambridge University Press, Cambridge, 1993.
[5] G. Casati, B. Chirikov, The Legacy of Chaos in Quantum Mechanics, Cambridge University Press, Cambridge, 1995, pp. 3–53.
[6] E. Ott, Chaos in Dynamical Systems, Cambridge University Press, Cambridge, 1993.
[7] H. Cerdeira, R. Ramaswamy, M. Gutzwiller, G. Casati (Eds.), Quantum Chaos, World Scientific, Singapore, 1991.
[8] G. Casati, Physica D 83 (1995) 59.
[9] M. Kollmann, H.W. Capel, Physica A 247 (1997) 379.
[10] L.E. Reichl, The Transition to Chaos in Conservative Classical Systems: Quantum Manifestation, Springer, Berlin, 1992.
[11] M.V. Berry, Proc. Roy. Soc. London A 413 183.
[12] J.Keating, in: T. Mullin (Ed.), The Nature of Chaos, Clarendon Press, Oxford, 1995, p. 282.
[13] L.D. Landau, E.M. Lifshitz, Quantum Mechanics. Non-relativistic Theory (Kvantovaja Mekhanika. Nereljativistskaja Teorija), Nauka, Moscow, 1984.
[14] V.I. Arnold, A. Avez, Ergodic Problems of Classical Mechanics, Benjamin, New York, 1968.
[15] R.L. Devaney, An Introduction to Chaotic Dynamical Systems, Addison-Wesley, Reading, MA, 1989.
[16] J.H. Hannay, M.V. Berry, Physica D 1 (1980) 267.
[17] J. Ford, G. Mantica, G.H. Ristow, Physica D 50 (1991) 493.
[18] J. Ford, G. Mantica, Am. J. Phys. 60 (12) (1992) 1086.
[19] B. Eckhardt, J. Phys. A 19 (1986) 1823.
[20] N.E. Hurt, Rev. Mod. Phys. 7 (1995) 103.
[21] J.P. Keating, Nonlinearity 4 (1991) 277.
[22] J.P. Keating, Nonlinearity 4 (1991) 309.
[23] I. Percival, F. Vivaldi, Physica D 25 (1987) 105.
[24] M. Bartuccelli, F. Vivaldi, Physica D 39 (1989) 194.
[25] M.D. Esposti, S. Graffi, S. Isola, Commun. Math. Phys. 167 (1995) 471.
[26] A. Bouzouina, S. De Bievre, Commun. Math. Phys. 178 (1996) 83.
[27] S. Knabe, J. Phys. A 23 (1990) 2013.
[28] N.L. Balazs, A. Voros, Ann. Phys. 190 (1989) 1.
[29] M. Saraceno, A. Voros, Physica D 79 (1994) 206.
[30] M. Saraceno, R.O. Vallejos, Chaos 6 (2) (1996) 193.
[31] M. Basilio de Matos, A.M. Ozorio de Almeida, Ann. Phys. 237 (1995) 46.
[32] A. Lakshminarayan, N.L. Balaz, Chaos, Solitons and Fractals 5 (1995) 1169.
[33] M. Saraceno, Ann. Phys. 199 (1990) 37.
[34] S. Nonnenmacher, 10 (1997) 1569.
[35] P. Pakonski, A. Ostruszka, K. Zyczkowski, Nonlinearity 12 (1999) 1.
[36] M. Toda, K. Ikeda, Phys. Lett. A 124 (1987) 165.
[37] S. Klimek, A. Lesniewsky, N. Maitra, R. Rubin, J. Math. Phys. 38 (1997) 67.
[38] S.P. Kuznetsov, Izv. Vuz. Prikl. Nelin. Dinam. 6 (3) (1998) 3.
[39] I.M. Gelfand, Dokl. Acad. Nauk SSSR 73 (1950) 1117.
[40] I.M. Gelfand, Mat. Prosv. (Gos. Izdat. Fiz. mat. Lit., Moscow) 5 (1995) 1169.
[41] S.P. Kuznetsov, Radiotekhnika i elektronika 23 (1980) 1104.
[42] P. Giblin, Primes and Programming, Cambridge University Press, Cambridge, 1993.
[43] T. Guhr, A. Müller-Groeling, H.A. Weidenmüller, Phys. Rep. 299 (1998) 189.
[44] O. Bohigos, M.J. Giannoni, C. Schmit, Phys. Rev. Lett. 52 (1984) 1.
[45] E.J. Heller, Phys. Rev. Lett. 53 (1984) 1515.
[46] L. Kaplan, Nonlinearity 12 (1999) R1.
[47] G.M. Zaslavsky, R.Z. Sagdeev, Introduction to Nonlinear Physics. From Pendulum to Turbulence and Chaos (Vvedenije v Nelineinuju Fiziku. ot Majatnika do Turbulentosti i Khaosa), Nauka, Moscow, 1988, p. 114.
[48] R. Bowen, Am. J. Math. 94 (1972) 413.
[49] J.M. Hammersley, D.C. Handscom, Monte Carlo Methods, London, NY, 1964.
[50] J.S. Bendat, A.G. Piersol, Random Data Analysis and Measurement Procedures, Wiley, New York, 1986.